Heme-Mediated Selection of Encapsulated *Streptococcus pneumoniae* in the Lungs by Oxidative Stress

Babek Alibayov[1], Ana G. Jop Vidal[1], Landon Murin[1], Anna Scasny[1], Kenichi Takeshita[1], Komal Beeton[1], Kristin S. Edwards[3], Tracy Punshon[4], Brian P. Jackson[4], Larry S. McDaniel[1,2], and Jorge E. Vidal[1,2,#],

[1]Department of Cell and Molecular Biology, [2]Center for Immunology and Microbial Research, [3]Department of Pharmacology and Toxicology, School of Medicine, University of Mississippi Medical Center, Jackson, MS. [4]Dartmouth College, Hanover New Hampshire.

Running title: Oxidative stress-mediated selection of encapsulated Spn

#Address correspondence to:

Jorge E. Vidal, PhD

2500 North State Street, Jackson Mississippi 39216

Phone : (601) 984-1711, Fax : (601) 984-1708

Email : jvidal@umc.edu

Abstract

Streptococcus pneumoniae (the pneumococcus) causes cytotoxicity and encapsulates within the lung parenchyma, leading to pneumococcal pneumonia. However, the underlying mechanisms remain unclear and likely involve multiple bacterial and host factors.

We investigated the selection process of encapsulated pneumococci, a critical factor in lung damage during pneumococcal pneumonia.

Our study revealed that pneumococci initially lack capsules but re-encapsulate upon reaching the alveoli. This process is driven by *S. pneumoniae*-derived hydrogen peroxide (Spn-H_2O_2), which oxidizes lung hemoglobin, leading to heme release and polymerized hemoglobin formation. Physiologically relevant levels of heme were found to promote the selection of encapsulated bacteria. Furthermore, encapsulation protects bacteria from intracellular heme toxicity, a defense absent in non-encapsulated strains. Ultrastructural analysis demonstrated interactions between hemoglobin and both encapsulated and non-encapsulated pneumococci in human sputum.

These findings reveal a critical connection between oxidative stress-mediated lung damage and the selection of encapsulated pneumococci, suggesting potential therapeutic avenues by targeting these oxidative processes.

36 **Introduction**

37 *Streptococcus pneumoniae* (Spn) strains colonize the lungs causing pneumonia, a global
38 disease that kills more than a million individuals every year.[1] Invasion of bronchi and terminal
39 bronchiole allows pneumococci to reach respiratory bronchiole, alveolar ducts, and alveoli, where
40 pneumococci have access to the alveolar-capillary network, a large surface area containing ~300
41 billion of capillaries and where the exchange of CO_2 by O_2 occurs.[2, 3]

42 In the lungs where molecular oxygen (O_2) is available, Spn uses a fermentative metabolism to
43 produce ATP by oxidizing glucose to acetate.[4, 5, 6] Spn strains encode an incomplete set of genes for
44 enzymes of the Krebs cycle, or proteins of the respiratory chain. ATP production includes the
45 oxidation of pyruvate by the enzyme pyruvate oxidase (SpxB), releasing H_2O_2 as a byproduct.[4, 5, 6] In
46 the absence of O_2, pyruvate is converted to L-lactate, whereas, in the presence of oxygen, L-lactate
47 is oxidized back to pyruvate, via lactate oxidase (LctO), producing H_2O_2 as a byproduct.[4, 5]

48 Besides components of the glycolytic pathway and atmospheric O_2, the alveolar-capillary
49 network is a source of erythrocytes and hemoglobin. We recently demonstrated that hemoglobin
50 enhances *in vitro* growth of Spn strains and upregulates expression of *spxB*.[7, 8] H_2O_2 produced by the
51 pneumococcus oxidizes oxy-hemoglobin (Fe^{2+}) from different mammals, including humans, to
52 produce the non-oxygen-binding form of hemoglobin known as met-hemoglobin (Hb-Fe^{3+}).[9, 10] The
53 oxidation of hemoglobin by Spn produced toxic species, including labile heme[11] and a hemoglobin-
54 derived tyrosyl radical [Fig. 1A, ($^{\bullet}$Hb-Fe^{4+})].[12] These toxic products are implicated in the
55 pathophysiology of human diseases characterized by intravascular hemolysis, such as sickle cell
56 disease (SCD), and in inflammatory conditions, such as sepsis.[13, 14, 15]

57 This study demonstrates that hydrogen peroxide produced by Spn (Spn-H_2O_2) oxidizes
58 hemoglobin within the alveolar-capillary network, driving the differentiation of encapsulated

59 pneumococci within the alveolar space. This oxidation process leads to hemoglobin polymerization,
60 which disrupts the alveolar epithelium and is closely associated with pneumococci. Ultrastructural
61 analysis of human sputum revealed interactions between hemoglobin and both encapsulated and
62 non-encapsulated pneumococci. Encapsulated, H_2O_2-producing pneumococci exhibit resistance to
63 physiological levels of free heme, unlike their unencapsulated, H_2O_2-deficient counterparts, which
64 are more susceptible to heme-mediated toxicity. These findings highlight the capsule's role as a
65 protective barrier against heme-mediated toxicity and suggest its potential as a therapeutic target
66 for pneumococcal pneumonia.
67
68 **Results**
69 **Spn oxidizes hemoglobin generating molecules of oxidative stress.** Reactive oxygen species (ROS)
70 can contribute to heme degradation by damaging the protoporphyrin IX ring (Fig. 1A)[16, 17, 18]. To
71 investigate Spn-H_2O_2 involvement in oxidative stress and hemoglobin oxidation, we assessed H_2O_2 in
72 Spn cultures. Wild-type Spn strains (TIGR4, D39, and EF3030) generated substantial H_2O_2 (>650 µM)
73 at 6 h post-inoculation in THY medium (Fig. 1B, and Fig. S1A) whereas the isogenic H_2O_2-defective
74 Δ*spxB*Δ*lctO* mutants did not (Fig. 1B and Fig. S1A). To further explore this, Spn and Δ*spxB*Δ*lctO*,
75 strains were cultured in THY supplemented with met-hemoglobin (THY-Hb^{3+}). Heme levels in
76 supernatants were quantified using an in-gel heme staining (Fig. S1B), and a Quantichrom assay.[19, 20]
77 Compared to the uninfected control, heme levels in Spn cultures were significantly reduced or
78 undetectable within 6 hours (Fig. 1C-E, Fig. S1C). In contrast, THY-Hb^{3+} cultures of Δ*spxB*Δ*lctO* strains
79 yielded >16.82 µM of total heme at 6 h (Fig. 1C-E). This heme degradation correlated with Spn-
80 mediated pseudoperoxidase activity, as Spn-H_2O_2 levels were undetectable in THY+Hb^{3+} cultures 2
81 or 4 h post-inoculation (Fig. 1F).

82 To confirm hemoglobin oxidation, we cultured TIGR4 and TIGR4Δ*spxB*Δ*lctO* in THY or in THY-
83 Hb^{3+} for two h. Subsequent metabolomic analysis using partial least squares discriminant analysis
84 (PLS-DA) revealed distinct metabolic profiles between groups (Fig. 1J). The largest biological
85 variation was observed between TIGR4 cultures grown in THY-Hb^{3+} (component 2, 10% variance;
86 AUC=0.9542) (Fig. 1K). A heatmap summarizing metabolites with at least a 2-fold change and FDR p-
87 value <0.05 is presented (Fig. 1J). Compared to THY cultures, TIGR4 grown with THY- Hb^{3+} exhibited
88 increased levels of metabolites indicative of hemoglobin oxidation, such as creatinine, isoleucine,
89 leucine, guanosine, putrescine, and tyrosyl. Conversely, aspartic acid, guanine, and oxoproline levels
90 decreased (Table S1). Interestingly, TIGR4 cultures with H_2O_2 (THY- Hb^{3+}) showed increased levels of
91 oxidative stress markers,[21] like methionine sulfoxide (MetO), oleamide, and putrescine (Table S1)
92 compared to Δ*spxB*Δ*lctO* mutant cultures. Additionally, methionine (precursor to MetO) and pyruvic
93 acid (SpxB substrate) were downregulated (Table S1). These findings collectively suggest that Spn-
94 derived H_2O_2 oxidizes hemoglobin and generating metabolites associated with oxidative stress.
95
96 **Spn oxidation and polymerization of hemoglobin favor the selection of encapsulated bacteria.**
97 Oxidation crosslinks hemoglobin globins, potentially leading to precipitation.[22, 23] Consistent with
98 this, Spn cultures in hemoglobin-supplemented media (THY-Hb^{3+}) exhibited reduced levels of soluble
99 α and β globins upon oxidation (Fig. 1G-H, Fig. S1D and, S1E). In contrast, H_2O_2-deficient mutants
100 displayed normal hemoglobin monomer and dimer levels in THY-Hb^{3+}, similar to uninfected controls
101 (Fig. 1G-H, Fig. S1D).
102 We next investigated the structural localization of the polymerized hemoglobin aggregates.
103 Confocal microscopy analysis of biofilms from Spn cultures grown in THY-Hb^{3+} included capsule,
104 hemoglobin, and DNA staining. Z-stack projections and their 3D reconstruction revealed bacteria

105 associated with hemoglobin (hereafter Spn-Hb$^+$) as early as 2 h post-inoculation, with increasing
106 abundance over time (Fig. 2A, Fig. S2A-B). Structures suggestive of hemoglobin polymers were also
107 observed (Fig. S2C and S2D). Additionally, Spn-Hb$^+$ bacteria were positive for staining with anti-alpha
108 chain hemoglobin antibodies (Not shown).

109 Confocal microscopy analysis revealed that a significant proportion of Spn-Hb$^+$ were non-
110 viable. Quantitative analysis of images showed only 12% of Hb$^+$-associated bacteria colocalized with
111 DNA (a viability marker), compared to 76% of capsular polysaccharide-positive (CPS$^+$) pneumococci
112 (Fig. 2B and not shown). Furthermore, the DNA area of Spn-Hb$^+$ bacteria was significantly smaller
113 than that of CPS$^+$ pneumococci (Fig. 2B), suggesting DNA degradation due to oxidative stress.
114 Notably, cultures with the H_2O_2-deficient Δ*spxB*Δ*lctO* strain showed a significant decrease in both
115 dead Spn-Hb$^+$ bacteria (Fig. 2C and 2D) and CPS$^+$ pneumococci (Fig. 2C). Similar trends were
116 observed in planktonic cultures, with wild-type exhibiting increased Spn-Hb$^+$ and reduced viability,
117 while the *ΔspxBΔlctO* mutant showed the opposite (Fig. 2E-G, S2F, S3A-C). These findings suggest
118 that oxidative products of hemoglobin, including heme (assessed in a later section), contribute to
119 bacterial toxicity.

120 The exclusive presence of Hb$^+$ bacteria in wild-type Spn cultures suggests hemoglobin binds
121 to the cell wall, followed by H_2O_2-mediated oxidation (Fig. 2H). To investigate heme location, we
122 quantified heme levels in cytosolic, insoluble and cell wall fractions of Spn grown with THY-Hb^{3+}.
123 Heme was detected in the insoluble fraction (Fig. 2J) and significantly increased in the cell wall
124 fraction of H_2O_2-deficient Δ*spxB*Δ*lctO* mutant compared to wild-type Spn (Fig. 2I). Conversely, the
125 cytosolic fraction of H_2O_2-producing Spn contained significantly more heme compared to the
126 Δ*spxB*Δ*lctO* mutant, indicating that hemoglobin oxidation facilitates heme uptake (Fig. 2K). These
127 findings demonstrate that Spn-H_2O_2-mediated hemoglobin oxidation contributes to bacterial killing,

128 hemoglobin polymerization, and the selection of encapsulated pneumococci, potentially enhancing
129 survival during infection.

130 **Spn-H_2O_2 oxidation of hemoglobin contributes to mortality in a mouse model of pneumococcal**
131 **disease.** Since hemorrhage, a hallmark of lobar pneumococcal pneumonia (also known as red
132 hepatization)[24], involves hemoglobin, we employed a mouse model to assess the contribution of
133 H_2O_2-mediated hemoglobin oxidation to pneumococcal pneumonia severity. The mouse model
134 mimics the natural course of infection, where Spn is aspirated into the lower airways, facilitating
135 colonization in the bronchi, bronchioles, and/or alveoli (Fig. 3A). Since the capsule *in vivo* protects
136 Spn from the immune response[2, 25, 26, 27], and mutations in *spxB* affect capsule production in some
137 strains[28], we quantified CPS^+ bacteria in strains used to inoculate animals (Fig. 3B). The majority of
138 TIGR4, TIGR4Ω*spxB-lctO,* D39, and D39Δ*spxB*Δ*lctO* (>84.1%) expressed the capsule, whereas the
139 capsule-deficient TIGR4Δ*cps* mutant and TIGR4Δ*spxB*Δ*lctO* exhibited significantly lower capsular
140 polysaccharide-positive (CPS^+) populations (<28.8%), compared to TIGR4 (Fig. 3C). Similar results
141 were obtained using an ELISA approach (Data not shown). Deletion of *spxB* and *lctO* affected
142 production of capsule in TIGR4 but not in D39, indicating strain-specific effects

143 Balb/c mice were then intranasally infected with wild-type strains (TIGR4 or D39) or H_2O_2-
144 deficient mutants. Mice infected with TIGR4, complemented TIGR4Ω*spxB-lctO,* or D39 succumbed
145 within 96 h post infection (Fig. 3D and Supplementary Fig. 4A, 5A). In contrast. mice infected with
146 TIGR4Δ*spxB*Δ*lctO* survived at least 96 h, and a significant proportion of mice infected with
147 D39Δ*spxB*Δ*lctO* also survived (Fig. 3D, and Supplementary Fig. 5A). Notably, D39-infected mice
148 succumbed 3.5 times faster than the D39Δ*spxB*Δ*lctO* group (not shown). Weight loss, another
149 indicator of disease severity, was also monitored. Animals infected with H_2O_2-producing strains

150 displayed significantly greater body weight reduction at the time of euthanasia compared to their
151 isogenic Δ*spxB*Δ*lctO* mutant counterpart (Fig. 3E, Supplementary Fig. 4B, and 5B).

152 Lung pathology in mice infected with TIGR4, or TIGR4Ω*spxB-lctO* resembled human lobar
153 pneumonia, exhibiting hemorrhage with focal sub-lobar lesions[24] (Fig. 3F). In contrast, lungs from
154 mice infected with H_2O_2-deficient strain appeared normal (Fig. 3F). This observation aligned with
155 bacterial burden data: the median lung density of TIGR4 reached $2.3x10^7$ cfu/g, while TIGR4Ω*spxB-*
156 *lctO* reached $1.4x10^8$ cfu/g (Fig. 3G, and Supplementary Fig. 4C). Importantly, the H_2O_2-deficient
157 strain was completely cleared from the lungs by 96 h post-infection (Fig. 3G). Consistent with lung
158 colonization, pneumococci were detected in the blood of mice infected with TIGR4, or TIGR4Ω*spxB-*
159 *lctO,* ($3.4x10^6$ and 2.8 $x10^6$ cfu/ml, respectively) (Fig. 3H) but not in those infected with H_2O_2-
160 deficient strain (Fig. 3H).

161 To investigate if the rapid clearance of the H_2O_2-deficient strain from the lung was due to
162 decreased adhesion, we infected human (A549), and mouse (MLE-12), alveolar type I pneumocytes
163 with TIGR4 or a GFP-tagged H_2O_2-deficient strain (TIGR4Δ*spxB*Δ*lctO*^{GFP}). Bacterial burden, quantified
164 by both culture and confocal microscopy, demonstrated comparable levels for both strains in both
165 human and mouse pneumocytes (Fig. 3I, 3J and 3K).

166

167 **Histopathological examination of lung tissue revealed extensive damage induced by H_2O_2-**
168 **producing pneumococci.** Mice infected with H_2O_2-producing strains, TIGR4 and D39, exhibited
169 severe lung pathology characterized by bronchiolar epithelial detachment, fibrotic alveolar changes,
170 alveolar hemorrhage, and pneumococcal infiltration (Fig. 3L, Supplementary Fig. 5D). Alveolar artery
171 endothelial damage was also evident in these mice. In contrast, H_2O_2-deficient strains,
172 TIGR4*ΔspxBΔlctO* and D39*ΔspxBΔlctO*, induced milder lung pathology with primarily inflammatory

173 cell infiltration and intimal/medial thickening of alveolar arteries, but without endothelial
174 cytotoxicity (Fig. 3L, Supplementary Fig. 5D). While TIGR4*ΔspxBΔlctO* caused minimal bronchiolar
175 hemorrhage and no fibrosis or cytotoxicity, D39*ΔspxBΔlctO* induced localized inflammation and
176 some alveolar fibrosis without endothelial damage (Fig. 3L and Supplementary Fig. 4E, and 5D).
177 Histopathological scoring revealed significantly higher scores for bronchiolar hypertrophy, cellular
178 exudate, and alveolar inflammatory cell infiltrate in lungs from mice infected with TIGR4 or
179 complemented TIGR4*ΩspxB-lctO* compared to those infected with TIGR4*ΔspxBΔlctO* (Fig. 3M-O).
180 These findings indicate that H_2O_2-producing pneumococci induce substantial cytotoxic damage
181 across multiple lung cell types.
182
183 **Increased reactive oxygen species in the lungs of mice infected with H_2O_2-producing pneumococci.**
184 To assess H_2O_2 production by pneumococci *in vivo*, we measured ROS levels in lung tissue. Mice
185 infected with wild-type TIGR4 for 24 h exhibited significantly elevated lung ROS levels compared to
186 uninfected mice or those infected with the H_2O_2-deficient Δ*spxB*Δ*lctO* strain (Fig. 3P), confirming
187 Spn-H_2O_2 production *in vivo*. While host immune cells such as neutrophils likely contribute to the
188 overall ROS levels, a human lung cell model was used to directly evaluate pneumococcus-derived
189 ROS. In this model, intracellular ROS in alveolar A549 cells infected with TIGR4 was significantly
190 elevated, mirroring the effect of menadione, a positive redox control (Supplementary Fig. 6A-B)[29].
191 Confocal microscopy confirmed intracellular pneumococci in both TIGR4 and *ΔspxBΔlctO* infected
192 cells (Supplementary Fig. 6C), suggesting H_2O_2 from TIGR4 contributed to the ROS rise. As H_2O_2
193 exposure can damage cellular structures, we examined potential damage to tubulin and GAPDH,
194 proteins known to be sensitive to H_2O_2[30, 31]. Western blotting revealed significant degradation of β-
195 tubulin and GAPDH in human alveolar cells infected with TIGR4 but not in those infected with the

196 H_2O_2-deficient *ΔspxBΔlctO*, while cytosolic catalase levels remained unchanged (Supplementary Fig.
197 6D-F). These findings demonstrate that Spn-H_2O_2 production elevates intracellular ROS levels,
198 leading to structural cellular damage.
199
200 ***In vivo* oxidation of hemoglobin by Spn-H_2O_2 selects for encapsulated pneumococci in the lung.**
201 Building on our *in vitro* observation that Spn-H_2O_2 oxidation of hemoglobin favors encapsulated
202 pneumococci, we investigated the lung subcellular compartments where this selection occurs. Lung
203 sections from mice infected with Spn were stained for capsule, DNA, and cell membranes, and
204 analyzed by confocal microscopy. Notably, within the open central channel (lumen) of respiratory
205 bronchioles in TIGR4-infected mice (Fig. 4A) or mice infected with the complemented TIGR4Ω*spxB-*
206 *lctO* strain (Fig. 4C), nearly all pneumococci (98%) lacked a capsule (referred to as decapsulated or D-
207 CPS) (Fig. 4D). Furthermore, D-CPS bacteria were the dominant population (88.4%) found inside the
208 bronchiolar epithelium (Fig. 4A, 4C-D, and Supplementary Fig. 7). The proportion of CPS^+
209 pneumococci increased significantly (by 42.1%) in Spn located within alveoli adjacent to bronchioles
210 (Fig. 4D).
211 In stark contrast to the bronchiolar environment, the proportion of CPS^+ pneumococci
212 increased significantly (by 39.5%) within the alveoli, while the lumen (central channel) showed a
213 marked decrease (Fig. 4A, 4C, and 4E). This trend continued as CPS^+ were 27.3% when bacteria
214 invaded the endothelial cells of pulmonary arteries (Fig. 4A and 4F). Notably, a similar pattern was
215 observed in D39-infected mice, with these CPS^+ bacteria concentrated on the bronchiolar membrane
216 and in alveoli adjacent to bronchioles (Supplementary Fig. 5E). Comparable findings were noted in
217 mice infected with serotype 3 strain WU-2 (data not shown). Since we began the experiment with a
218 population of CPS^+ pneumococci infected into the animals (Fig. 3B), these findings suggest that the

219 bacteria lose their capsule (decapsulate) during bronchiolar invasion and then regain it (re-
220 encapsulate) as they migrate deeper into the lung reaching the alveolar epithelium (Fig. 4G).

221 Motivated by the abundance of hemoglobin in the alveolar-capillary network, we
222 investigated how its oxidation affects capsular gene expression. Incubating pneumococci (Spn) with
223 red blood cells (RBCs), adding RBCs to alveolar cells, or bronchial cells all significantly increased
224 transcription of *cps4A*, the first gene in the capsule locus, and *spxB* (Fig. 4H and 4J). Spectroscopic
225 analysis of culture supernatants confirmed methemoglobin formation (heme-Fe^{3+}) in Spn-infected
226 RBCs-containing cultures, where most heme was already degraded (Fig. 4I). Importantly, only the
227 higher concentration (10 µM) of hemoglobin mimicked the upregulation observed with RBCs (Fig. 4H
228 and 4J), suggesting a dose-dependent effect. Previous studies reported similar findings, Spn grown
229 in hemoglobin, mouse model of pneumonia but not in a carriage model, exhibited upregulated *spxB*
230 and *cps* locus genes (Fig. 4K, Supplementary Fig. 6G). Notably, genes encoding pyruvate node
231 enzymes (*lctO, ackA, ldh*) and the pneumolysin gene *ply* remained unaffected by hemoglobin
232 exposure (Fig. 4K, Supplementary Fig. 6G). Similarly, ply expression remained unchanged in the
233 H_2O_2-deficient TIGR4ΔspxBΔlctO mutant compared to wild-type TIGR4 under hemoglobin
234 exposure[32].

235

236 **Hemoglobin polymerization occurs in the lung during pneumococcal disease.** We then investigated
237 hemoglobin oxidation *in vivo*. Since hemoglobin oxidation can lead to its aggregation, we examined
238 lung sections from Spn-infected animals for the presence of aggregated hemoglobin. We discovered
239 aggregated hemoglobin, red blood cells (RBCs), CPS^+ pneumococci, and bacteria associated with
240 hemoglobin (Spn-Hb^+) within alveoli (Fig. 5A, and Supplementary Fig. 8), the alveolar lumen (not
241 shown), and the pulmonary artery (Fig. 5D). In contrast, mice infected with the H_2O_2-deficient

242 TIGR4*ΔspxBΔlctO* strain did not exhibit aggregated hemoglobin or Spn-Hb$^+$ bacteria in the alveoli
243 (Fig. 5B) or pulmonary arteries (Fig. 5C). To assess the potential toxic effect of hemoglobin oxidation
244 on Spn, we quantified the DNA area in both CPS$^+$ pneumococci and Spn-Hb$^+$ bacteria. The DNA area
245 associated with Spn-Hb$^+$ bacteria was significantly lower compared to that of CPS$^+$ pneumococci (Fig.
246 5E), suggesting that hemoglobin oxidation may impair bacterial survival.

247 In alveoli with extensive hemoglobin polymerization, we observed nuclei resembling those of
248 white blood cells (leukocytes), but no nuclei from other cell types such as type I and II pneumocytes
249 or endothelial cells were present (Fig. 5A, Supplementary Fig. 8). To confirm that these were
250 leukocytes migrating after tissue damage, lung sections were stained with an anti-CD45 antibody
251 (Fig. 5F). This revealed that a majority of the cells (median, 56%) were CD45$^+$, indicating immune
252 cells. Compared to nuclear area of CD45$^+$ cells, the nuclear area of these CD45$^-$ cells was significantly
253 shrunken, suggesting cytotoxicity (Fig. 5G).

254 We then examined pneumococci in close proximity, within ~1 µm, to CD45$^+$ cells (Fig. 5H).
255 The area of both the DNA (Fig. 5I) and capsule (Fig. 5J) of CPS$^+$ pneumococci near CD45$^+$ cells was
256 similar to those of bacteria farther away in the alveoli. This suggests that capsule expression was not
257 directly influenced by the presence of immune cells.

258 Since hemoglobin oxidation in the alveoli leads to heme degradation and iron release[11, 33],
259 we expected elevated iron levels in the lungs. Using high-resolution laser ablation inductively
260 coupled plasma time-of-flight mass spectrometry (LA-ICP-TOFMS), we quantified iron levels in lung
261 sections from infected and uninfected mice. These analyses revealed high iron concentrations in
262 animals infected with H_2O_2-producing pneumococci, with iron localized in areas exhibiting tissue
263 damage (Fig. 5K, Supplementary Fig. 9). In contrast, mice infected with the H_2O_2-deficient
264 TIGR4*ΔspxBΔlctO* strain only displayed increased iron levels in areas with abundant inflammatory

265 infiltrate (Supplementary Fig. 9). These findings collectively demonstrate that *in vivo* hemoglobin
266 oxidation triggers its polymerization, facilitates the formation of Spn-Hb$^+$ pneumococci, and
267 promotes bacterial encapsulation.

268 Next, hemoglobin oxidation was investigated in sputum from a pneumococcal pneumonia
269 patient[34]. Ultrastructural analysis revealed aggregation of CPS$^+$ pneumococci embedded in the
270 sputum sample (Fig. 5L) and presence of Spn-Hb$^+$ bacteria throughout (Fig. 5M). Hemoglobin signal
271 was detected surrounding encapsulated bacteria, as quantified by overlap volume analysis. Due to
272 bacterial embedding within the aggregate, hemoglobin-capsule interactions were significantly
273 reduced compared to capsule-DNA interaction (Fig. 5N). Furthermore, hemoglobin overlap with
274 DNA from Spn-Hb$^+$ bacteria was significantly lower than that from CPS$^+$ pneumococci (Fig. 5O),
275 suggesting hemoglobin-induced toxicity in Spn-Hb$^+$ bacteria.

276

277 **Both H_2O_2 and the capsule protect pneumococci from heme toxicity.** Since heme exposure can kill
278 a subpopulation of pneumococci, we investigated the mechanisms of heme resistance. Minimum
279 bactericidal concentration (MBC) assays revealed that ≥10 µM heme was needed to kill 99.97% of
280 wild-type pneumococci (Fig. 6A, Fig. 6E, Fig. 6G, and Supplementary Fig. 10A). Culture supernatants
281 from pneumococci surviving exposure to lower heme concentrations (≤7.5 µM) showed significant
282 heme degradation, while cultures exposed to a lethal dose (12.5 µM) retained the characteristic
283 heme peak in spectral analysis (Fig. 6C and 6D). These findings suggest that pneumococci can
284 degrade heme at low concentrations, potentially protecting themselves from its toxic effects. Labile
285 heme levels in the bloodstream and lungs are ~0.2 µM[35, 36, 37]. Therefore, H_2O_2 production by
286 pneumococci might be particularly important for defense against heme toxicity at these
287 physiological concentrations.

288 To directly test this hypothesis, we performed heme susceptibility assays in cultures lacking
289 H_2O_2 production. H_2O_2-defective strains (*ΔspxBΔlctO*) were significantly more susceptible to heme,
290 with an MBC below 2.5 µM (Fig. 6B, Fig. 6F and Supplementary Fig. 10B). Similarly, treating wild-type
291 pneumococci with catalase, an enzyme that degrades H_2O_2, also rendered them susceptible to 2.5
292 µM heme (Fig. 6J). Spectral analysis confirmed the presence of intact heme in supernatants from
293 cultures lacking H_2O_2 (Fig. 6C).

294 We then explored whether the pneumococcal capsule contributes to heme resistance, in
295 addition to the established role of H_2O_2 production. Capsule-deficient strains (TIGR4Δ*cps* and R6)
296 displayed increased heme susceptibility compared to wild-type strains (MBC of 5 µM for mutants vs.
297 >10 µM for wild-type) despite producing normal H_2O_2 levels (Fig. 1B, 6K-L, and Supplementary Fig.
298 1A). Furthermore, scavenging H_2O_2 with catalase in these capsule-deficient strains dramatically
299 reduced the MBC of heme to 1.25 µM or 0.625 µM, respectively (Fig. 6K and 6L).

300 To assess labile heme as a defense strategy, mice were infected with a heme-susceptible
301 pneumococcal strain (TIGR4*ΔspxBΔlctO*) after depletion of complement factor 3 (C3) using cobra
302 venom factor (CoVF). C3 depletion increases susceptibility to bloodstream infections[38]. We reasoned
303 that if heme offered protection, CoVF-treated mice would still be resistant (Suppl. Fig. 4D). While
304 some CoVF-treated mice lost weight (Suppl. Fig. 4E), likely due to CoVF itself, and as per protocol
305 were euthanized and considered in the mortality group (Suppl. Fig. 4F), there were no significant
306 differences in bacterial colonization or dissemination compared to controls (Suppl. Fig. 4G).

307 Collectively, these *in vivo* and *in vitro* experiments demonstrate that both the capsule and
308 H_2O_2 production contribute to pneumococcal heme resistance (Fig. 6M). Loss of either factor
309 increases heme susceptibility, and the absence of both renders pneumococci highly susceptible to
310 heme toxicity at concentrations below 1.5 µM (Fig. 6M).

311

312 **Discussion**

313 Spn thrives in the lung's alveolar-capillary network, exploiting host oxygen, carbohydrates,
314 and iron from heme-hemoglobin. However, this study demonstrates that Spn's aerobic metabolism
315 releases H_2O_2, unintentionally causing host damage. *In vitro*, Spn-H_2O_2 reacts with Fe^{2+}, generating
316 hydroxyl radicals ($^{\bullet}OH^{-}$)[39, 40] and oxidizes hemoproteins (hemoglobin, cytochrome C) to labile heme
317 and tyrosyl radicals[9, 11, 12]. Our findings reveal these Spn-H_2O_2 driven oxidative reactions as a major
318 contributor to lung toxicity. Additionally, neutrophil infiltration in response to pneumococcal
319 infection[41] produces hydrogen peroxide, potentially synergizing with Spn-H_2O_2 to exacerbate
320 oxidation of heme-containing proteins within the alveolar-capillary microenvironment. Hemoglobin
321 oxidation triggers cytosolic protein degradation and facilitates Spn differentiation into encapsulated
322 bacteria, primarily within alveoli and pulmonary artery endothelial cells. These mechanisms
323 represent novel targets for intervention against pneumococcal disease, which claims millions of lives
324 annually.

325 Spn-H_2O_2 oxidation of hemoglobin induces globin chain aggregation (α and β) under
326 physiological infection conditions, potentially aiding pneumococcal suspension in lung tissue[22, 23].
327 This contrasts with *in vitro* studies reporting preferential crosslinking of either α or β globin by H_2O_2.
328 The oxidation also generates methionine sulfoxide (MetOH) in the β chain, potentially contributing
329 to globin collapse[23]. Free hemoglobin is normally bound by haptoglobin (Hp) for macrophage uptake
330 via CD163 receptors. However, oxidized hemoglobin exhibits reduced Hp binding, weakening its
331 interaction with macrophages[22, 42]. In our mouse model, oxidized hemoglobin bound to a subset of
332 non-encapsulated Spn-Hb^{+} bacteria, while the majority localized near PMNs. This suggests

333 membrane-bound hemoglobin in Spn-Hb$^+$ bacteria trigger an immune response, supported by the
334 abundance of CD45$^+$ leukocytes surrounding Spn-Hb$^+$ in severe pneumonia.

335 Pneumolysin (Ply), a pneumococcal toxin, may not fully explain the complex lung pathology
336 observed in pneumonia[43, 44, 45, 46, 47, 48]. Spn-H_2O_2 shows promise as a mediator of both cell death and
337 pneumococcal disease in animal models[28, 45, 49, 50, 51, 52]. Notably, the co-activation of apoptosis and
338 pyroptosis markers suggests a multifaceted cytotoxicity mechanism[53, 54, 55, 56]. Our study identified a
339 loss of cellular structure in mouse lung regions exhibiting severe alveolar and bronchial cytotoxicity,
340 harboring intracellular pneumococci. Notably, epithelial cell nuclear DNA was absent, while
341 infiltrated CD45$^+$ cells retained nuclei. *In vivo* cytotoxicity was partially attributed to Spn-H_2O_2
342 produced by pneumococci in the lungs. Furthermore, Spn-H_2O_2 was delivered intracellularly to
343 cultured human alveolar cells. While Spn-H_2O_2 can directly oxidize proteins, LA-ICP-TOFMS analysis
344 revealed elevated iron levels in these cytotoxic regions. This suggests a potential role for the Fenton
345 reaction in generating hydroxyl radicals ($^{\bullet}OH^-$) and subsequent DNA damage, contributing to the
346 observed toxicity[40, 57].

347 Our study unveils a mechanism linking H_2O_2-producing pneumococci to lung cell death and
348 structural collapse. Infection of human alveolar or bronchial cells with these bacteria triggered the
349 degradation of key cytoskeletal proteins (β-tubulin, β-actin) and cytosolic GAPDH (glycolysis) [12, 31].
350 This correlated with microtubule collapse and cell swelling, potentially mimicking damage observed
351 in cardiomyocytes exposed to high H_2O_2[30]. Mechanistically, Spn-H_2O_2 likely targets cysteine residues
352 in α and β-globin chains, weakening tubulin-tubulin interactions and inhibiting polymerization[30, 58,
353 59]. Similarly, H_2O_2 can directly oxidize the catalytic cysteine (Cys152) of GAPDH, leading to S-
354 glutathionylation and subsequent cell death[31, 60, 61]. This process holds therapeutic potential, as
355 studies suggest pharmacological induction of GAPDH oxidation shows promise for treating tumors[62].

356 Furthermore, antioxidant treatment in animal models and human trials improves survival rates from
357 pneumococcal infections[63, 64, 65].

358 Spn-H_2O_2 oxidation of hemoglobin triggers a cascade of detrimental events within the lung.
359 This process releases heme, leading to its degradation and the formation of highly reactive tyrosyl
360 radicals[12, 17, 18, 66, 67]. Heme destruction is well-documented for its toxicity. For instance, the
361 accumulation of labile heme during hemolytic diseases like malaria and sickle cell disease (SCD) is
362 linked to inflammation, blood clot formation (prothrombotic complications), and a form of cell
363 death called PANoptosis[15, 68, 69]. Importantly, the oxidation of other heme-containing proteins like
364 myoglobin, cytochrome C (Cytc), and methemoglobin (Hb-Fe3+) also generates these toxic tyrosyl
365 radicals[12, 70, 71, 72, 73]. Collectively, our findings unveil novel intervention strategies. By addressing
366 oxidative reactions in pneumococcal pneumonia or by stimulating the natural antioxidant response
367 of lung cells through pharmacological approaches, we may unlock promising therapeutic
368 possibilities.

369

370 **Material and Methods**

371 The Materials and Methods section is provided in supplementary materials. It can be
372 accessed online for further details.

373

374 **Acknowledgements**

375 This study was supported in part by grants from the National Institutes of Health including
376 R21AI144571, 1R01AI175461-01A1 (JEV). BA was supported by a Fulbright scholarship awarded by
377 the US Department of State. Studies of confocal microscopy, histology, and Oroboros O2k
378 FluoRespirometry, were supported by grants from the National Institute of General Medical

379 Sciences (NIGMS) of the National Institutes of Health under Award Numbers P20GM121334 and
380 P20GM104357. JEV is also supported by a grant from NIGMS through the Molecular Center of
381 Health and Disease (1P20GM144041-01A1 7651). Laser ablation elemental imaging was performed
382 at the Dartmouth Biomedical National Elemental Imaging Resource (BNEIR) supported by NIGMS
383 R24GM141194. RNA-seq data analysis was performed through the UMMC Molecular and Genomics
384 Facility is supported, in part, by funds from the NIGMS, including the Molecular Center of Health and
385 Disease-COBRE (P20GM144041), Mississippi INBRE (P20GM103476) and Obesity, Cardiorenal and
386 Metabolic Diseases- COBRE (P30GM149404) and Mississippi Center of Perinatal Research
387 (1P20GM121334). The content is solely the responsibility of the authors and does not necessarily
388 represent the official view of the NIH or the US Department of State. We thank Drs. Poonam
389 Sharma, William Daley, and Timothy Allen from the Department of Pathology at the University of
390 Mississippi Medical Center (UMMC) for providing the human sputum sample, and Dr. Allen for
391 assistance with pathology scoring. We also appreciate the assistance of Dr. Antonino Baez (UMMC)
392 for CPS purification and Jorge M. Vidal (UMMC) for conducting experiments with serotype 3 strains.

393

394 **References**

395 1. Wahl, B. *et al.* Burden of Streptococcus pneumoniae and Haemophilus influenzae type b
396 disease in children in the era of conjugate vaccines: global, regional, and national estimates
397 for 2000-15. *Lancet Glob Health* **6**, e744-e757 (2018).

398

399 2. Weiser, J.N., Ferreira, D.M. & Paton, J.C. Streptococcus pneumoniae: transmission,
400 colonization and invasion. *Nat Rev Microbiol* **16**, 355-367 (2018).

401

402 3. Musher, D.M. & Thorner, A.R. Community-acquired pneumonia. *N Engl J Med* **371**, 1619-
403 1628 (2014).

404

405 4. Lisher, J.P. *et al.* Biological and Chemical Adaptation to Endogenous Hydrogen Peroxide
406 Production in Streptococcus pneumoniae D39. *mSphere* **2** (2017).

407

408 5. Taniai, H. *et al.* Concerted action of lactate oxidase and pyruvate oxidase in aerobic growth
409 of Streptococcus pneumoniae: role of lactate as an energy source. *J Bacteriol* **190**, 3572-3579
410 (2008).

411

412 6. Tettelin, H. *et al.* Complete genome sequence of a virulent isolate of Streptococcus
413 pneumoniae. *Science* **293**, 498-506 (2001).

414

415 7. Akhter, F. *et al.* Hemoglobin induces early and robust biofilm development in Streptococcus
416 pneumoniae by a pathway that involves comC but not the cognate comDE two-component
417 system. *Infect Immun* (2021).

418

419 8. Akhter, F. *et al.* Hemoglobin stimulates vigorous growth of Streptococcus pneumoniae and
420 shapes the pathogen's global transcriptome. *Sci Rep* **10**, 15202 (2020).

421

422 9. McDevitt, E. *et al.* Hydrogen Peroxide Production by Streptococcus pneumoniae Results in
423 Alpha-hemolysis by Oxidation of Oxy-hemoglobin to Met-hemoglobin. *mSphere* **5** (2020).

424

425 10. Kajfasz, J.K. *et al.* Two Spx proteins modulate stress tolerance, survival, and virulence in
426 Streptococcus mutans. *J Bacteriol* **192**, 2546-2556 (2010).

427

428 11. Alibayov, B. *et al.* Oxidative Reactions Catalyzed by Hydrogen Peroxide Produced by
429 Streptococcus pneumoniae and Other Streptococci Cause the Release and Degradation of
430 Heme from Hemoglobin. *Infect Immun* **90**, e0047122 (2022).

431

432 12. Scasny, A. *et al.* Oxidation of hemoproteins by Streptococcus pneumoniae collapses the cell
433 cytoskeleton and disrupts mitochondrial respiration leading to cytotoxicity of human lung
434 cells. *bioRxiv* (2023).

435

436 13. Nader, E., Romana, M. & Connes, P. The Red Blood Cell-Inflammation Vicious Circle in Sickle
437 Cell Disease. *Front Immunol* **11**, 454 (2020).

438

439 14. Buehler, P.W., Humar, R. & Schaer, D.J. Haptoglobin Therapeutics and Compartmentalization
440 of Cell-Free Hemoglobin Toxicity. *Trends Mol Med* **26**, 683-697 (2020).

441

442 15. Kato, G.J., Steinberg, M.H. & Gladwin, M.T. Intravascular hemolysis and the pathophysiology
443 of sickle cell disease. *J Clin Invest* **127**, 750-760 (2017).

16. Maitra, D. *et al.* Reaction of hemoglobin with HOCl: mechanism of heme destruction and free iron release. *Free Radic Biol Med* **51**, 374-386 (2011).

17. Nagababu, E. & Rifkind, J.M. Heme degradation by reactive oxygen species. *Antioxid Redox Signal* **6**, 967-978 (2004).

18. Nagababu, E. & Rifkind, J.M. Formation of fluorescent heme degradation products during the oxidation of hemoglobin by hydrogen peroxide. *Biochem Biophys Res Commun* **247**, 592-596 (1998).

19. Pamplona, A. *et al.* Heme oxygenase-1 and carbon monoxide suppress the pathogenesis of experimental cerebral malaria. *Nat Med* **13**, 703-710 (2007).

20. Mingone, C.J. *et al.* Protoporphyrin IX generation from delta-aminolevulinic acid elicits pulmonary artery relaxation and soluble guanylate cyclase activation. *Am J Physiol Lung Cell Mol Physiol* **291**, L337-344 (2006).

21. Moskovitz, J. & Smith, A. Methionine sulfoxide and the methionine sulfoxide reductase system as modulators of signal transduction pathways: a review. *Amino Acids* **53**, 1011-1020 (2021).

22. Vallelian, F. *et al.* The reaction of hydrogen peroxide with hemoglobin induces extensive alpha-globin crosslinking and impairs the interaction of hemoglobin with endogenous scavenger pathways. *Free Radic Biol Med* **45**, 1150-1158 (2008).

23. Jia, Y., Buehler, P.W., Boykins, R.A., Venable, R.M. & Alayash, A.I. Structural basis of peroxide-mediated changes in human hemoglobin: a novel oxidative pathway. *J Biol Chem* **282**, 4894-4907 (2007).

24. Zinserling, V.A., Swistunov, V.V., Botvinkin, A.D., Stepanenko, L.A. & Makarova, A.E. Lobar (croupous) pneumonia: old and new data. *Infection* **50**, 235-242 (2022).

25. Brissac, T. *et al.* Capsule Promotes Intracellular Survival and Vascular Endothelial Cell Translocation during Invasive Pneumococcal Disease. *mBio* **12**, e0251621 (2021).

26. Hyams, C., Camberlein, E., Cohen, J.M., Bax, K. & Brown, J.S. The Streptococcus pneumoniae capsule inhibits complement activity and neutrophil phagocytosis by multiple mechanisms. *Infect Immun* **78**, 704-715 (2010).

483
484 27. Kim, J.O. *et al.* Relationship between cell surface carbohydrates and intrastrain variation on
485 opsonophagocytosis of Streptococcus pneumoniae. *Infect Immun* **67**, 2327-2333 (1999).

486
487 28. Echlin, H. *et al.* Pyruvate Oxidase as a Critical Link between Metabolism and Capsule
488 Biosynthesis in Streptococcus pneumoniae. *PLoS pathogens* **12**, e1005951 (2016).

489
490 29. Criddle, D.N. *et al.* Menadione-induced reactive oxygen species generation via redox cycling
491 promotes apoptosis of murine pancreatic acinar cells. *J Biol Chem* **281**, 40485-40492 (2006).

492
493 30. Goldblum, R.R. *et al.* Oxidative stress pathogenically remodels the cardiac myocyte
494 cytoskeleton via structural alterations to the microtubule lattice. *Dev Cell* **56**, 2252-2266
495 e2256 (2021).

496
497 31. Hildebrandt, T., Knuesting, J., Berndt, C., Morgan, B. & Scheibe, R. Cytosolic thiol switches
498 regulating basic cellular functions: GAPDH as an information hub? *Biol Chem* **396**, 523-537
499 (2015).

500
501 32. Alibayov, B. *et al.* Oxidative Reactions Catalyzed by Hydrogen Peroxide Produced by
502 Streptococcus pneumoniae and Other Streptococci Cause the Release and Degradation of
503 Heme from Hemoglobin. *Infect Immun*, e0047122 (2022).

504
505 33. Womack, E., Alibayov, B., Vidal, J.E. & Eichenbaum, Z. Endogenously produced H(2)O(2) is
506 intimately involved in iron metabolism in Streptococcus pneumoniae. *Microbiol Spectr* **12**,
507 e0329723 (2024).

508
509 34. Vidal, A.G.J. *et al.* Fluorescent antibody-based detection and ultrastructural analysis of
510 Streptococcus pneumoniae in human sputum. *Pneumonia (Nathan)* **17**, 4 (2025).

511
512 35. Adisa, O.A. *et al.* Association between plasma free haem and incidence of vaso-occlusive
513 episodes and acute chest syndrome in children with sickle cell disease. *Br J Haematol* **162**,
514 702-705 (2013).

515
516 36. Reiter, C.D. *et al.* Cell-free hemoglobin limits nitric oxide bioavailability in sickle-cell disease.
517 *Nat Med* **8**, 1383-1389 (2002).

518
519 37. Saltini, C. *et al.* Lung microhaemorrhage drives oxidative/inflammatory damage in alpha(1)-
520 antitrypsin deficiency. *ERJ Open Res* **9** (2023).

521

522 38. Lokken-Toyli, K.L. *et al.* Impaired upper respiratory tract barrier function during postnatal
523 development predisposes to invasive pneumococcal disease. *PLoS Pathog* **20**, e1012111
524 (2024).

525
526 39. Wu, X. *et al.* Interaction between Streptococcus pneumoniae and Staphylococcus aureus
527 Generates (.)OH Radicals That Rapidly Kill Staphylococcus aureus Strains. *J Bacteriol* **201**
528 (2019).

529
530 40. Imlay, J.A., Chin, S.M. & Linn, S. Toxic DNA damage by hydrogen peroxide through the Fenton
531 reaction in vivo and in vitro. *Science* **240**, 640-642 (1988).

532
533 41. Taenaka, H. *et al.* Neutrophil reduction attenuates the severity of lung injury in the early
534 phase of pneumococcal pneumonia in mice. *Am J Physiol Lung Cell Mol Physiol* **327**, L141-
535 L149 (2024).

536
537 42. Ginzburg, Y., An, X., Rivella, S. & Goldfarb, A. Normal and dysregulated crosstalk between
538 iron metabolism and erythropoiesis. *Elife* **12** (2023).

539
540 43. Nishimoto, A.T., Rosch, J.W. & Tuomanen, E.I. Pneumolysin: Pathogenesis and Therapeutic
541 Target. *Front Microbiol* **11**, 1543 (2020).

542
543 44. Shak, J.R. *et al.* Novel role for the Streptococcus pneumoniae toxin pneumolysin in the
544 assembly of biofilms. *mBio* **4**, e00655-00613 (2013).

545
546 45. Rubins, J.B. *et al.* Toxicity of pneumolysin to pulmonary alveolar epithelial cells. *Infect Immun*
547 **61**, 1352-1358 (1993).

548
549 46. Rubins, J.B., Duane, P.G., Charboneau, D. & Janoff, E.N. Toxicity of pneumolysin to pulmonary
550 endothelial cells in vitro. *Infect Immun* **60**, 1740-1746 (1992).

551
552 47. van der Poll, T. & Opal, S.M. Pathogenesis, treatment, and prevention of pneumococcal
553 pneumonia. *Lancet* **374**, 1543-1556 (2009).

554
555 48. Gonzales, J. *et al.* Streptococcus pneumoniae and Its Virulence Factors H(2)O(2) and
556 Pneumolysin Are Potent Mediators of the Acute Chest Syndrome in Sickle Cell Disease.
557 *Toxins (Basel)* **13** (2021).

558
559 49. Shenoy, A.T. *et al.* Streptococcus pneumoniae in the heart subvert the host response through
560 biofilm-mediated resident macrophage killing. *PLoS pathogens* **13**, e1006582 (2017).

50. Brissac, T., Shenoy, A.T., Patterson, L.A. & Orihuela, C.J. Cell invasion and pyruvate oxidase derived H2O2 are critical for Streptococcus pneumoniae mediated cardiomyocyte killing. *Infection and immunity* (2017).

51. Ramos-Montanez, S. *et al.* Polymorphism and regulation of the spxB (pyruvate oxidase) virulence factor gene by a CBS-HotDog domain protein (SpxR) in serotype 2 Streptococcus pneumoniae. *Mol Microbiol* **67**, 729-746 (2008).

52. Spellerberg, B. *et al.* Pyruvate oxidase, as a determinant of virulence in Streptococcus pneumoniae. *Mol Microbiol* **19**, 803-813 (1996).

53. Rai, P. *et al.* Streptococcus pneumoniae secretes hydrogen peroxide leading to DNA damage and apoptosis in lung cells. *Proc Natl Acad Sci U S A* **112**, E3421-3430 (2015).

54. Surabhi, S. *et al.* Hydrogen Peroxide Is Crucial for NLRP3 Inflammasome-Mediated IL-1beta Production and Cell Death in Pneumococcal Infections of Bronchial Epithelial Cells. *J Innate Immun* **14**, 192-206 (2022).

55. Brissac, T., Shenoy, A.T., Patterson, L.A. & Orihuela, C.J. Cell Invasion and Pyruvate Oxidase-Derived H(2)O(2) Are Critical for Streptococcus pneumoniae-Mediated Cardiomyocyte Killing. *Infect Immun* **86** (2018).

56. Feldman, C. *et al.* The effects of pneumolysin and hydrogen peroxide, alone and in combination, on human ciliated epithelium in vitro. *Respir Med* **96**, 580-585 (2002).

57. Park, S., You, X. & Imlay, J.A. Substantial DNA damage from submicromolar intracellular hydrogen peroxide detected in Hpx- mutants of Escherichia coli. *Proc Natl Acad Sci U S A* **102**, 9317-9322 (2005).

58. Landino, L.M., Hagedorn, T.D., Kim, S.B. & Hogan, K.M. Inhibition of tubulin polymerization by hypochlorous acid and chloramines. *Free Radic Biol Med* **50**, 1000-1008 (2011).

59. Clark, H.M., Hagedorn, T.D. & Landino, L.M. Hypothiocyanous acid oxidation of tubulin cysteines inhibits microtubule polymerization. *Arch Biochem Biophys* **541**, 67-73 (2014).

60. Magherini, F. *et al.* Protein expression profiles in Saccharomyces cerevisiae during apoptosis induced by H2O2. *Proteomics* **7**, 1434-1445 (2007).

600 61. Mustafa Rizvi, S.H. *et al.* Oxidized GAPDH transfers S-glutathionylation to a nuclear protein
601 Sirtuin-1 leading to apoptosis. *Free Radic Biol Med* **174**, 73-83 (2021).

602

603 62. Ma, E. *et al.* Pharmacologic ascorbate induces neuroblastoma cell death by hydrogen
604 peroxide mediated DNA damage and reduction in cancer cell glycolysis. *Free Radic Biol Med*
605 **113**, 36-47 (2017).

606

607 63. Carlson, D., Maass, D.L., White, D.J., Tan, J. & Horton, J.W. Antioxidant vitamin therapy alters
608 sepsis-related apoptotic myocardial activity and inflammatory responses. *Am J Physiol Heart*
609 *Circ Physiol* **291**, H2779-2789 (2006).

610

611 64. Remy, K.E. *et al.* Haptoglobin improves shock, lung injury, and survival in canine pneumonia.
612 *JCI Insight* **3** (2018).

613

614 65. Janz, D.R. *et al.* Association between cell-free hemoglobin, acetaminophen, and mortality in
615 patients with sepsis: an observational study. *Crit Care Med* **41**, 784-790 (2013).

616

617 66. Nagababu, E. & Rifkind, J.M. Reaction of hydrogen peroxide with ferrylhemoglobin:
618 superoxide production and heme degradation. *Biochemistry* **39**, 12503-12511 (2000).

619

620 67. Nagababu, E. & Rifkind, J.M. Heme degradation during autoxidation of oxyhemoglobin.
621 *Biochem Biophys Res Commun* **273**, 839-845 (2000).

622

623 68. Sundaram, B. *et al.* NLRP12-PANoptosome activates PANoptosis and pathology in response
624 to heme and PAMPs. *Cell* (2023).

625

626 69. Hopp, M.T. & Imhof, D. Linking Labile Heme with Thrombosis. *J Clin Med* **10** (2021).

627

628 70. Gunther, M.R. *et al.* Site-specific spin trapping of tyrosine radicals in the oxidation of
629 metmyoglobin by hydrogen peroxide. *Biochem J* **330 (Pt 3)**, 1293-1299 (1998).

630

631 71. Shumaev, K.B., Kosmachevskaya, O.V., Timoshin, A.A., Vanin, A.F. & Topunov, A.F. Dinitrosyl
632 iron complexes bind with hemoglobin as markers of oxidative stress. *Methods Enzymol* **436**,
633 445-461 (2008).

634

635 72. Barr, D.P., Gunther, M.R., Deterding, L.J., Tomer, K.B. & Mason, R.P. ESR spin-trapping of a
636 protein-derived tyrosyl radical from the reaction of cytochrome c with hydrogen peroxide. *J*
637 *Biol Chem* **271**, 15498-15503 (1996).

638

639 73. Qian, S.Y. *et al.* Identification of protein-derived tyrosyl radical in the reaction of cytochrome
640 c and hydrogen peroxide: characterization by ESR spin-trapping, HPLC and MS. *Biochem J*
641 **363**, 281-288 (2002).

642

643

644 **Figure legends**

645 **Fig. 1. Oxidation of hemoglobin by Spn creates metabolites that contributes to oxidative stress.** (A)
646 Schematic representation of oxy-hemoglobin (Hb^{2+}), met-hemoglobin (Hb^{3+}), and ferryl-hemoglobin ($\bullet Hb^{4+}$).
647 (B) Spn was cultured in THY medium at 37°C for 6 h. Supernatants were collected, and H_2O_2 concentration
648 was quantified using Amplex Red (LOD < 0.56 μM). (C) THY added with met-hemoglobin (THY-Hb^{3+}) was
649 inoculated with Spn or left uninfected. Supernatants, THY alone, or Hb^{3+} (10 μM) were analyzed by native gel
650 electrophoresis with in-gel heme staining. (D & E) Heme, or (F) H_2O_2, was quantified in supernatants from (C)
651 using the QuantiChrom Heme Assay or Amplex Red assays, respectively. (G) Supernatants from cultures in (C)
652 and Hb^{3+} (10 μM) were analyzed by Western blot with a mouse monoclonal anti-β-hemoglobin antibody. (H)
653 Densitometric analysis of Hb monomer relative to control Hb^{3+}. Data in panels B, D-F, and H represent mean ±
654 SEM from ≥ 3 independent experiments. Statistical significance was determined by one-way ANOVA with
655 Dunnett's post hoc test (*p < 0.05, **p < 0.001, ***p < 0.0005, ****p < 0.0001). (I) Heatmap depicting
656 pairwise comparisons between groups for identified molecules. Each row represents a chemical compound,
657 and each column represents a comparison. Asterisks indicate statistical significance by Mann-Whitney U test.
658 The color bar indicates the chemical superclass. (J) PCA biplot showing the first two principal components
659 with group membership and normal data ellipses. (K) PLS-DA biplots of the first two components, showing
660 group membership and normal data ellipses.

661 **Fig. 2. Oxidation of hemoglobin by Spn selects for hemoglobin-binding (Spn-Hb^{+}) and encapsulated**
662 **pneumococci.** TIGR4 (A, B, E) or TIGR4Δ*spxB*Δ*lctO* (C) were incubated with Hb^{3+} and analyzed. Biofilms (A, C)
663 or planktonic bacteria (E) were stained for capsule (green), Hb (red), and DNA (blue). Images were acquired
664 by confocal microscopy and represent z-stack projections. Arrows: white, CPS^{+} bacteria; yellow, Spn-Hb^{+}

665 bacteria; arrowheads, DNA. (B) Area occupied by CPS^+ and Spn-Hb^+ bacteria was quantified using Imaris
666 software. The top panel shows masks used for quantification. (D) Minimum fluorescent intensity (MFI) of Spn-
667 Hb^+ bacteria (red channel) in TIGR4 (A) or TIGR4Δ*spxB*Δ*lctO* (C) cultures incubated for 6 h was measured with
668 Imaris software. (F) TIGR4 or TIGR4Δ*spxB*Δ*lctO* were incubated with Hb for 6 h. Planktonic bacteria were
669 collected, stained for Hb and DNA, and analyzed by confocal microscopy. XY, XZ (bottom), and YZ (side)
670 optical sections are shown. (G) MFI of the DAPI channel (live Spn) was measured using Imaris software. (H)
671 Schematic diagram depicting the hypothesized mechanism: Hb binds a cell wall receptor, is oxidized by Spn-
672 H_2O_2, releasing heme that enters the cytosol. (J, K) Spn was incubated with Hb for 4 h. Cellular fractionation
673 was performed, and the insoluble fraction is shown in (J). Heme was quantified from the (I) cell wall fraction
674 or the (K) cytosolic fraction using the QuantiChrom Heme Assay. Data (B, D, G, I, K) are presented as mean ±
675 SEM of at least three independent experiments. Statistical analysis: Student's t-test (B, D, G) or one-way
676 ANOVA with Dunnet's test for multiple comparisons (I, K). ns, not significant; *, $p < 0.05$; ***, $p < 0.005$; **, p
677 < 0.0001.

678 **Fig. 3. Pneumococci lacking capsule and hydrogen peroxide are rapidly cleared from the lungs.** (A)
679 Schematic representation of the murine pneumococcal pneumonia model. (B) Confocal micrographs of
680 capsule-stained pneumococci. (C) Quantification of capsule production (percentage capsule-positive
681 bacteria). (D-H) Groups of eight Balb/c mice were intranasally inoculated with approximately ~10^7 colony-
682 forming units (CFU) of the indicated strain. Survival (D) and weight loss (E) were monitored. At endpoint, lung
683 tissues were harvested, imaged (F), homogenized to quantify bacterial burden (G), and processed for
684 histological analysis (L). Blood was collected for bacterial quantification (H). (I) Human alveolar A549 (J) or
685 mouse alveolar MLE-12 (J) cells were infected with TIGR4 or $TIGR4^{GFP}$Δ*spxB*Δ*lctO* for 6 hours, followed by
686 bacterial enumeration. (K) Confocal microscopy of membrane-, DNA-, and capsule-stained A549 cells infected
687 with pneumococci. (M-O) Lung sections were subjected to histopathological analysis, and scores for
688 bronchiolar hypertrophy (M), bronchiolar cellular exudate (N), and alveolar inflammatory cell infiltrate (O)
689 were assigned by a blinded pathologist. (P) Hydrogen peroxide levels in lung homogenates from mock-

690 infected or pneumococcus-infected mice. Data are presented as mean ± SD. One-way ANOVA with Dunnett's
691 multiple comparisons test was used for (C, E, G, H, M-P), and Mann-Whitney test for (I, J). Survival analysis
692 was performed using the log-rank Mantel-Cox test. *p<0.0001, **p<0.01, ***p<0.001, ****p<0.0001. ns: not
693 significant.

694 **Fig. 4. *S. pneumoniae* producing hydrogen peroxide encapsulates in the alveolar epithelium.** Balb/c mice
695 were intranasally infected with TIGR4 (~10^7 CFU) (A, D-F), TIGR4Δ*spxB*Δ*lctO* (B), or complemented
696 TIGR4Ω*spxB-lctO* (C) and euthanized when moribund or at 96 h post-infection. Lung sections were stained for
697 cell membrane, capsule, and DNA. Confocal microscopy was used to image bronchioles, alveoli, and
698 pulmonary arteries and z-stack projections were obtained. Encapsulated (CPS^+) and de-capsulated (D-CPS)
699 pneumococci are indicated. A region of interest (ROI) was defined to delineate lumen and cellular
700 compartments. DAPI and capsule fluorescence intensity, and CPS^+ or D-CPS pneumococcal population density
701 (% Spn) were quantified in bronchioles (D), alveoli (E), and arteries (F) of TIGR4-infected mice. (G) Schematic
702 depicting the hypothesized transition of CPS^+ pneumococci from bronchioles to alveoli, involving de-
703 capsulation (D-CPS) for bronchiolar invasion and subsequent re-encapsulation in the alveolar epithelium. (H-J)
704 TIGR4 was cultured in THY (no cells), alveolar A549, or bronchial Calu-3 cells, with red blood cells (RBC), or in
705 THY supplemented with hemoglobin (Hb). RNA was extracted, and *cps4A* (H) and *spxB* (J) gene transcription
706 was analyzed. Hb release in THY-RBC cultures infected with TIGR4 (RBC Spn-infected) was assessed by
707 spectroscopy (I), with indicated wavelengths for oxy-hemoglobin (Heme-Fe^{2+}) and met-hemoglobin (Heme-
708 Fe^{3+}). (K) Heatmap visualization compares gene expression levels. Genes analyzed include those encoding
709 pyruvate node enzymes, pneumolysin (*ply*) and capsule locus genes. Samples are from D39 cultures grown on
710 THY-Hb^{3+} (Hemoglobin) vs. THY, THY-Hb^{3+} incubated for 2 h vs. 1 h and from *In vivo* TIGR4-infection model of
711 invasive pneumococcal disease (IPD) compared with gene expression in the nasopharynx. Analysis was
712 performed using the Mann Whitney test (D-F) and the non-parametric Wilcox test in (K) ns= not significant,
713 *p<0.05, **p<0.01, ***p<0.001.

714 **Fig. 5. *In vivo* hemoglobin oxidation selects for encapsulated pneumococci.** (A-D, F-H) Lung sections from
715 Balb/c mice infected with TIGR4 or TIGR4Δ*spxB*Δ*lctO* were immunostained for hemoglobin, capsule, DNA
716 and/or $CD45^+$. Confocal microscopy z-stack projections of alveoli (A, B, and F) and pulmonary arteries (C and
717 D) are shown. Red blood cells (RBC), leukocytes (Leuk), encapsulated (CPS^+), de-capsulated (D-CPS) bacteria,
718 hemoglobin-bound pneumococci ($Spn\text{-}Hb^+$), and $CD45^+$ leukocytes are indicated. (E) Quantification of DNA
719 area within CPS^+ and $Spn\text{-}Hb^+$ pneumococci in alveoli using Imaris software. Confocal micrographs (F) were
720 used to generate (G) 3D masks for $CD45^+$ and $CD45^-$ cells, CPS^+ and D-CPS pneumococci using Imaris software.
721 (H) Nuclear area in $CD45^+$ and $CD45^-$ cells. (I) DNA area and (J) capsule area within CPS^+ pneumococci, in close
722 proximity (~1 µm) to $CD45^+$ cells, or farther and classified as alveolar pneumococci. At least three lungs from
723 infected animals were analyzed. Micrographs and quantitative data are presented from a representative
724 animal. (K) Elemental mapping of $^{56}Fe^+$ in lung sections by LA-ICP-TOF-MS, with iron accumulation indicated
725 by arrows. (L-O) Human sputum stained for hemoglobin, pneumococcal capsule and DNA. (L) Confocal optical
726 XY middle section and corresponding XZ (underneath), and YZ (side) sections; (M) enlarged region. (N)
727 Overlap volume analysis of the capsule and DNA and capsule and hemoglobin. (O) Overlap volume analysis of
728 hemoglobin (Hb) and DNA from CPS+ and hemoglobin and DNA from non-encapsulated bacteria (D-CPS).
729 Statistical significance was determined using the Mann Whitney test (E, G, I, J); ns= not significant,
730 ****$p<0.0001$.

731 **Fig. 6. Hydrogen peroxide and the capsule protects pneumococci against heme toxicity.** TIGR4 (A),
732 TIGR4Δ*spxB*Δ*lctO* (B), D39 (E), or D39Δ*spxB*Δ*lctO* (F) were incubated with or without heme (4 h). Bacterial
733 density was measured. Supernatants from heme challenge [(5 µM), C] or [(12.5 µM), D] were collected for
734 spectral analysis. (G) EF3030 or EF3030Δ*spxB*Δ*lctO* were cultured in a 96-well plate with heme-supplemented
735 THY and incubated overnight. NC: uninfected THY; PC: untreated THY with pneumococci. TIGR4 (J), TIGR4Δ*cps*
736 (K), or R6 (L) were cultured in heme supplemented THY with or without catalase (400 U/mL). Cultures were
737 incubated (4 h) and density measured by dilution and plating. (M) Proposed model for capsule and H_2O_2
738 protection against heme toxicity. Limit of detection (LOD) <50 CFU/mL. Data represent the mean ± SEM of

739 two technical replicates from three independent experiments. Statistical analysis: Mann-Whitney U test was
740 used to compare Soret peak absorbance (405 nm) between uninfected and pneumococci-infected media (B-
741 D); (A, E, F, J-L) One-way ANOVA with Dunnett's multiple comparison test. ns: not significant, *: $p < 0.05$, **: p
742 < 0.01.
743
744

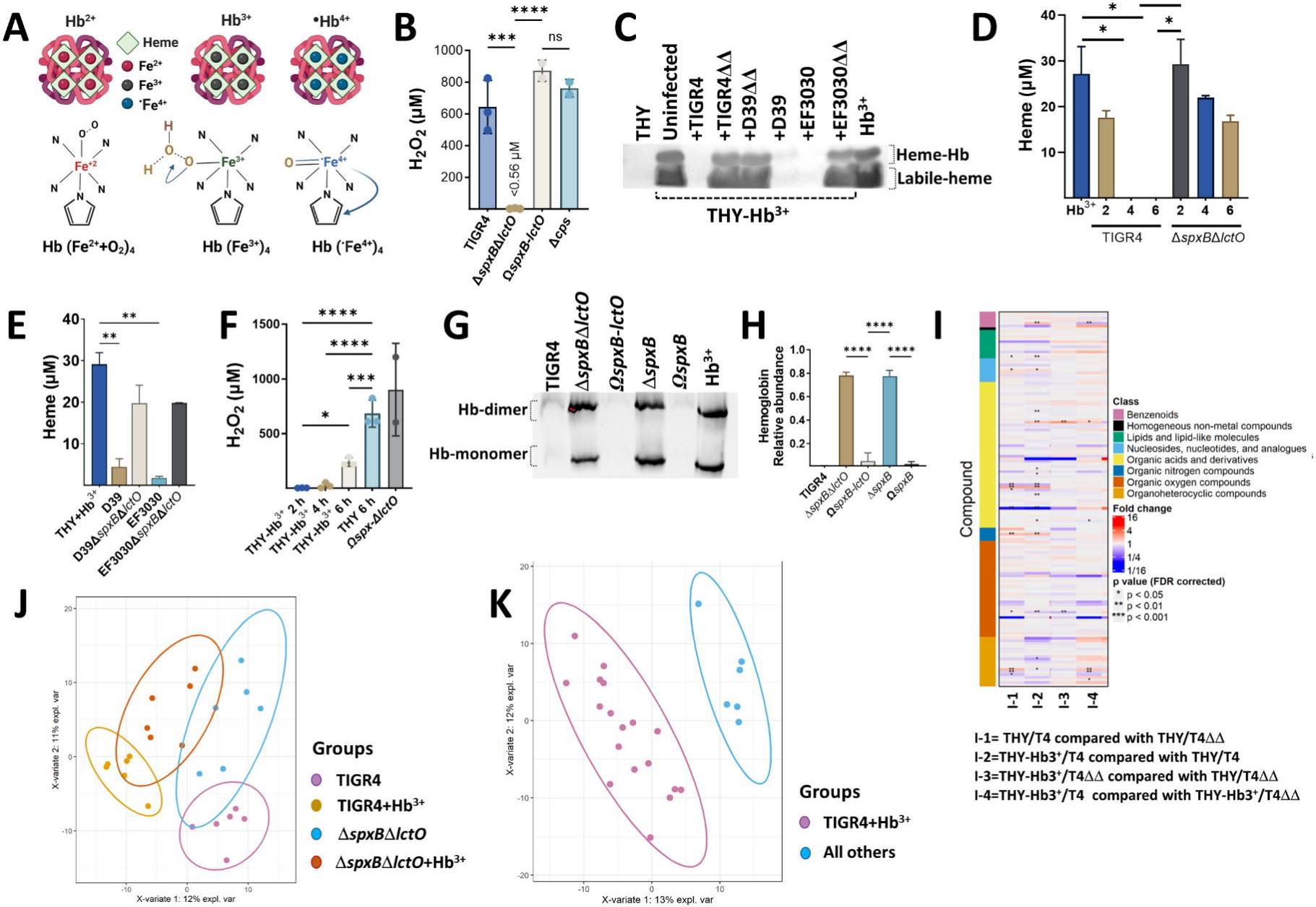
A
Hb2+
Hb3+
•Hb4+
Heme
Fe2+
Fe3+
•Fe4+
Hb (Fe2++O2)4
Hb (Fe3+)4
Hb (•Fe4+)4
B
H2O2 (µM)
<0.56 µM
TIGR4
ΔspxBΔlctO
ΩspxB-lctO
Δcps
C
THY
Uninfected
+TIGR4
+TIGR4ΔΔ
+D39ΔΔ
+D39
+EF3030
+EF3030ΔΔ
Hb3+
Heme-Hb
Labile-heme
THY-Hb3+
D
Heme (µM)
Hb3+
TIGR4
ΔspxBΔlctO
E
Heme (µM)
THY+Hb 3+
D39
D39ΔspxBΔlctO
EF3030
EF3030ΔspxBΔlctO
F
H2O2 (µM)
THY-Hb 3+ 2 h
THY-Hb 3+ 4 h
THY-Hb 3+ 6 h
THY 6 h
Ωspx-ΔlctO
G
TIGR4
ΔspxBΔlctO
ΩspxB-lctO
ΔspxB
ΩspxB
Hb3+
Hb-dimer
Hb-monomer
H
Hemoglobin Relative abundance
TIGR4
ΔspxBΔlctO
ΩspxB-lctO
ΔspxB
ΩspxB
I
Compound
Class
Benzenoids
Homogeneous non-metal compounds
Lipids and lipid-like molecules
Nucleosides, nucleotides, and analogues
Organic acids and derivatives
Organic nitrogen compounds
Organic oxygen compounds
Organoheterocyclic compounds
Fold change
16
4
1
1/4
1/16
p value (FDR corrected)
* p < 0.05
** p < 0.01
*** p < 0.001
I-1
I-2
I-3
I-4
I-1= THY/T4 compared with THY/T4ΔΔ
I-2=THY-Hb3+/T4 compared with THY/T4
I-3=THY-Hb3+/T4ΔΔ compared with THY/T4ΔΔ
I-4=THY-Hb3+/T4 compared with THY-Hb3+/T4ΔΔ
J
X-variate 1: 12% expl. var
X-variate 2: 11% expl. var
Groups
TIGR4
TIGR4+Hb3+
ΔspxBΔlctO
ΔspxBΔlctO+Hb3+
K
X-variate 1: 13% expl. var
X-variate 2: 12% expl. var
Groups
TIGR4+Hb3+
All others

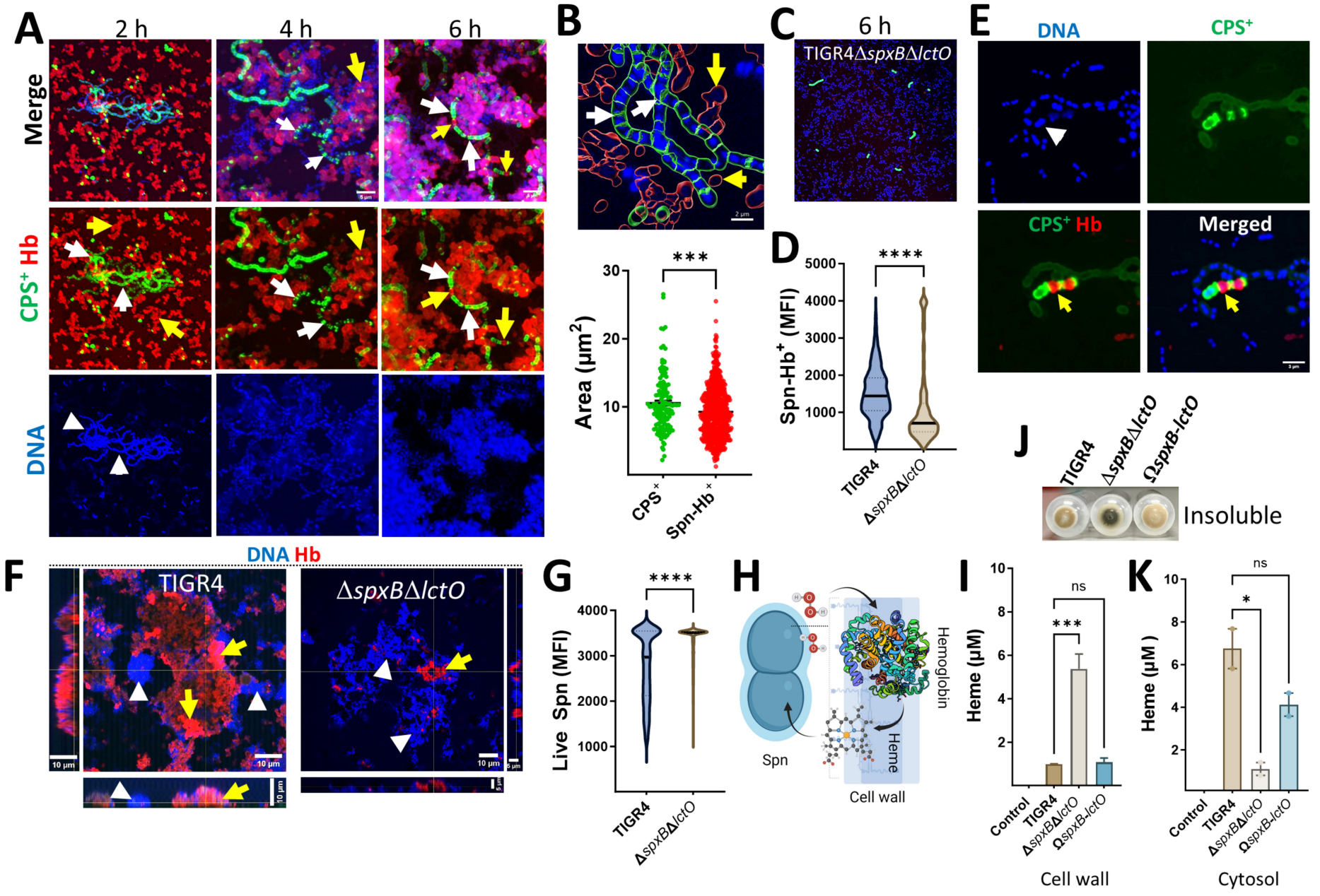
A
2 h
4 h
6 h
Merge
CPS+ Hb
DNA
B
Area (μm2)
***
CPS+
Spn-Hb+
C
6 h
TIGR4ΔspxBΔlctO
D
Spn-Hb+ (MFI)
****
TIGR4
ΔspxBΔlctO
E
DNA
CPS+
CPS+ Hb
Merged
F
DNA Hb
TIGR4
ΔspxBΔlctO
G
Live Spn (MFI)
****
TIGR4
ΔspxBΔlctO
H
Spn
Heme
Hemoglobin
Cell wall
I
Heme (μM)
ns
***
Control
TIGR4
ΔspxBΔlctO
ΩspxB-lctO
Cell wall
J
TIGR4
ΔspxBΔlctO
ΩspxB-lctO
Insoluble
K
Heme (μM)
ns
*
Control
TIGR4
ΔspxBΔlctO
ΩspxB-lctO
Cytosol

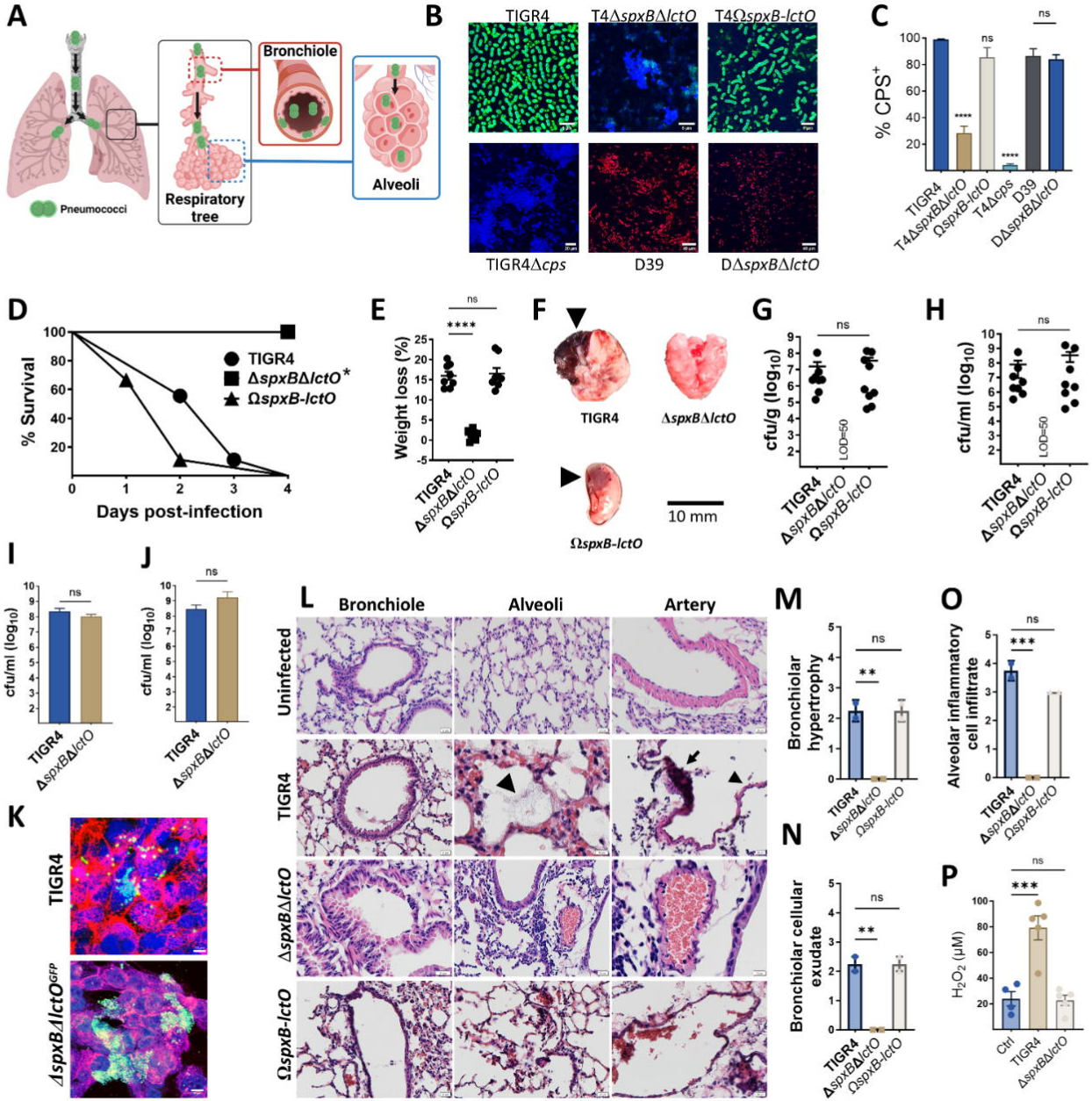
A
Pneumococci
Respiratory tree
Bronchiole
Alveoli
B
TIGR4
T4ΔspxBΔlctO
T4ΩspxB-lctO
TIGR4Δcps
D39
DΔspxBΔlctO
C
% CPS+
ns
****
TIGR4
T4ΔspxBΔlctO
ΩspxB-lctO
T4Δcps
D39
DΔspxBΔlctO
D
% Survival
Days post-infection
TIGR4
ΔspxBΔlctO*
ΩspxB-lctO
E
Weight loss (%)
ns
****
F
TIGR4
ΔspxBΔlctO
ΩspxB-lctO
10 mm
G
cfu/g (log10)
ns
LOD=50
H
cfu/ml (log10)
ns
LOD=50
I
cfu/ml (log10)
ns
J
cfu/ml (log10)
ns
K
TIGR4
ΔspxBΔlctOGFP
L
Bronchiole
Alveoli
Artery
Uninfected
TIGR4
ΔspxBΔlctO
ΩspxB-lctO
M
Bronchiolar hypertrophy
ns
**
N
Bronchiolar cellular exudate
ns
**
O
Alveolar inflammatory cell infiltrate
ns
***
P
H2O2 (μM)
ns
***
Ctrl
TIGR4
ΔspxBΔlctO

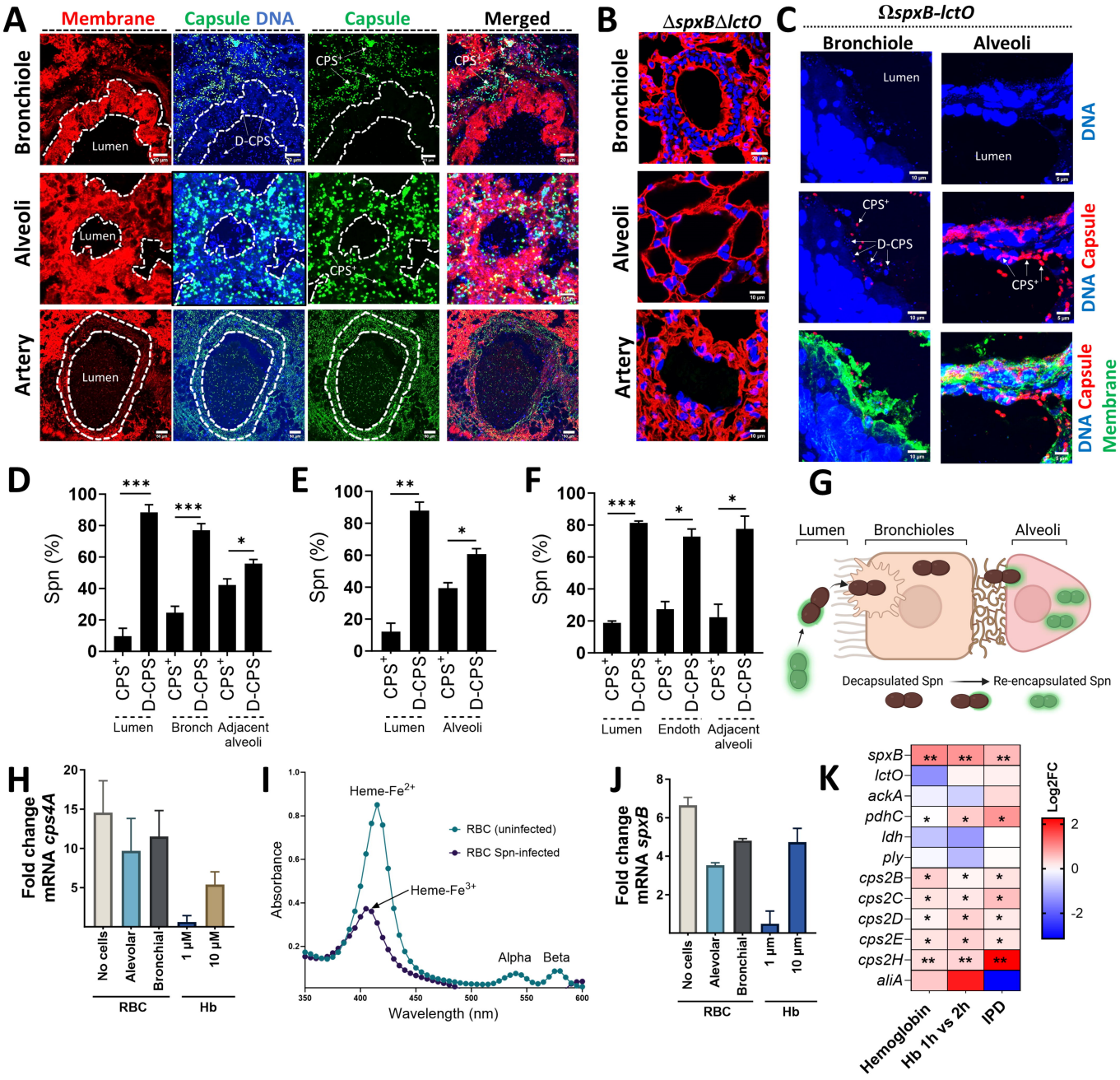
A
Membrane
Capsule DNA
Capsule
Merged
Bronchiole
Alveoli
Artery
Lumen
D-CPS
CPS+
B
ΔspxBΔlctO
C
ΩspxB-lctO
Bronchiole
Alveoli
DNA
DNA Capsule
DNA Capsule Membrane
D
Spn (%)
CPS+
D-CPS
Lumen
Bronch
Adjacent alveoli
E
Alveoli
F
Endoth
G
Lumen
Bronchioles
Alveoli
Decapsulated Spn
Re-encapsulated Spn
H
Fold change mRNA cps4A
No cells
Alevolar
Bronchial
1 µM
10 µM
RBC
Hb
I
Heme-Fe2+
Heme-Fe3+
RBC (uninfected)
RBC Spn-infected
Absorbance
Alpha
Beta
Wavelength (nm)
J
Fold change mRNA spxB
K
spxB
lctO
ackA
pdhC
ldh
ply
cps2B
cps2C
cps2D
cps2E
cps2H
aliA
Log2FC
Hemoglobin
Hb 1h vs 2h
IPD

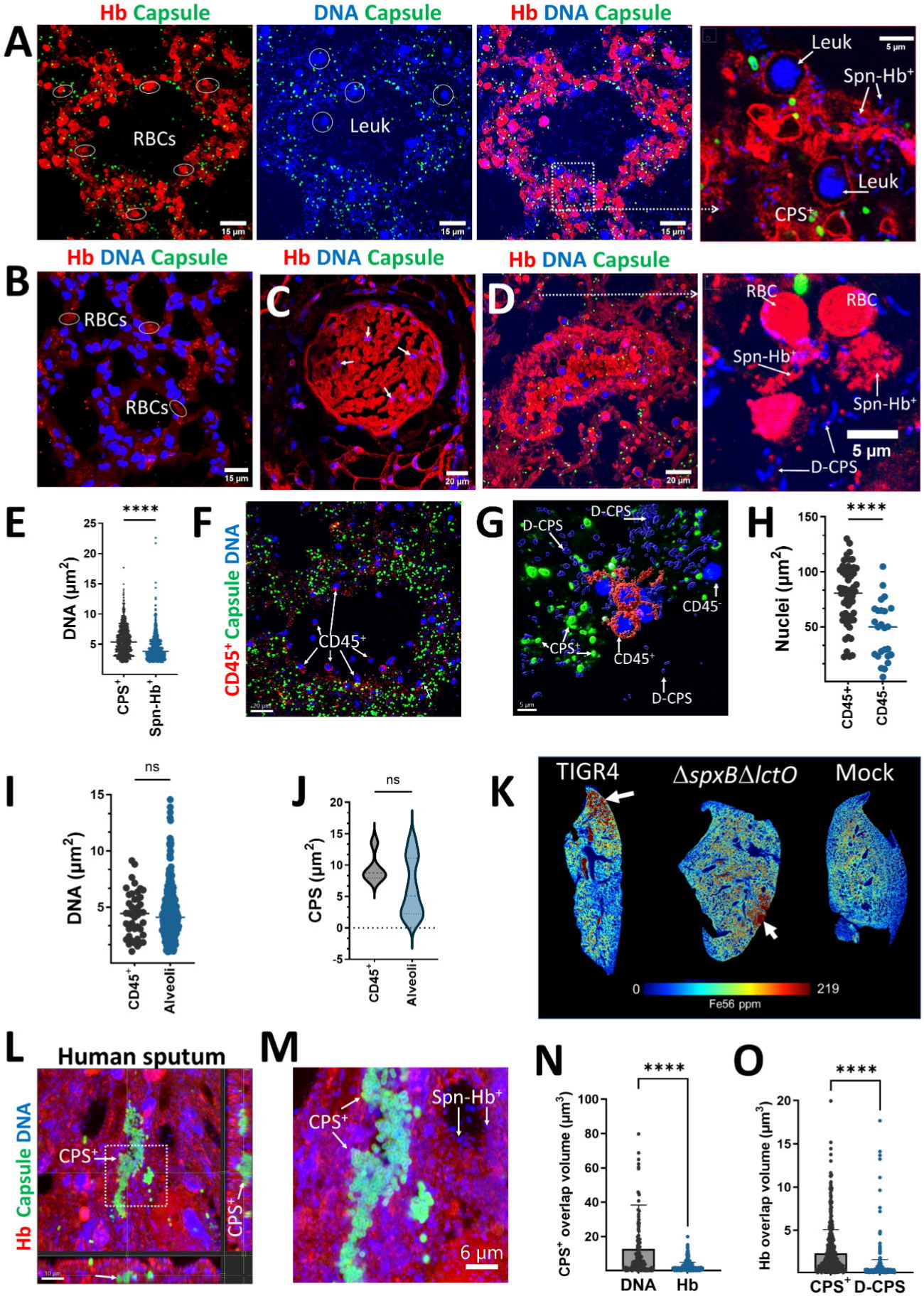
A
Hb Capsule
DNA Capsule
Hb DNA Capsule
RBCs
Leuk
Leuk
Spn-Hb+
Leuk
CPS+
15 µm
5 µm
B
Hb DNA Capsule
RBCs
RBCs
C
Hb DNA Capsule
D
Hb DNA Capsule
RBC
RBC
Spn-Hb+
Spn-Hb+
D-CPS
5 µm
20 µm
E
****
DNA (µm2)
CPS+
Spn-Hb+
F
CD45+ Capsule DNA
CD45+
G
D-CPS
D-CPS
CD45-
CPS+
CD45+
D-CPS
H
****
Nuclei (µm2)
CD45+
CD45-
I
ns
DNA (µm2)
CD45+
Alveoli
J
ns
CPS (µm2)
CD45+
Alveoli
K
TIGR4
ΔspxBΔlctO
Mock
0
219
Fe56 ppm
L
Human sputum
Hb Capsule DNA
CPS+
CPS+
M
CPS+
Spn-Hb+
6 µm
N
****
CPS+ overlap volume (µm3)
DNA
Hb
O
****
Hb overlap volume (µm3)
CPS+ D-CPS

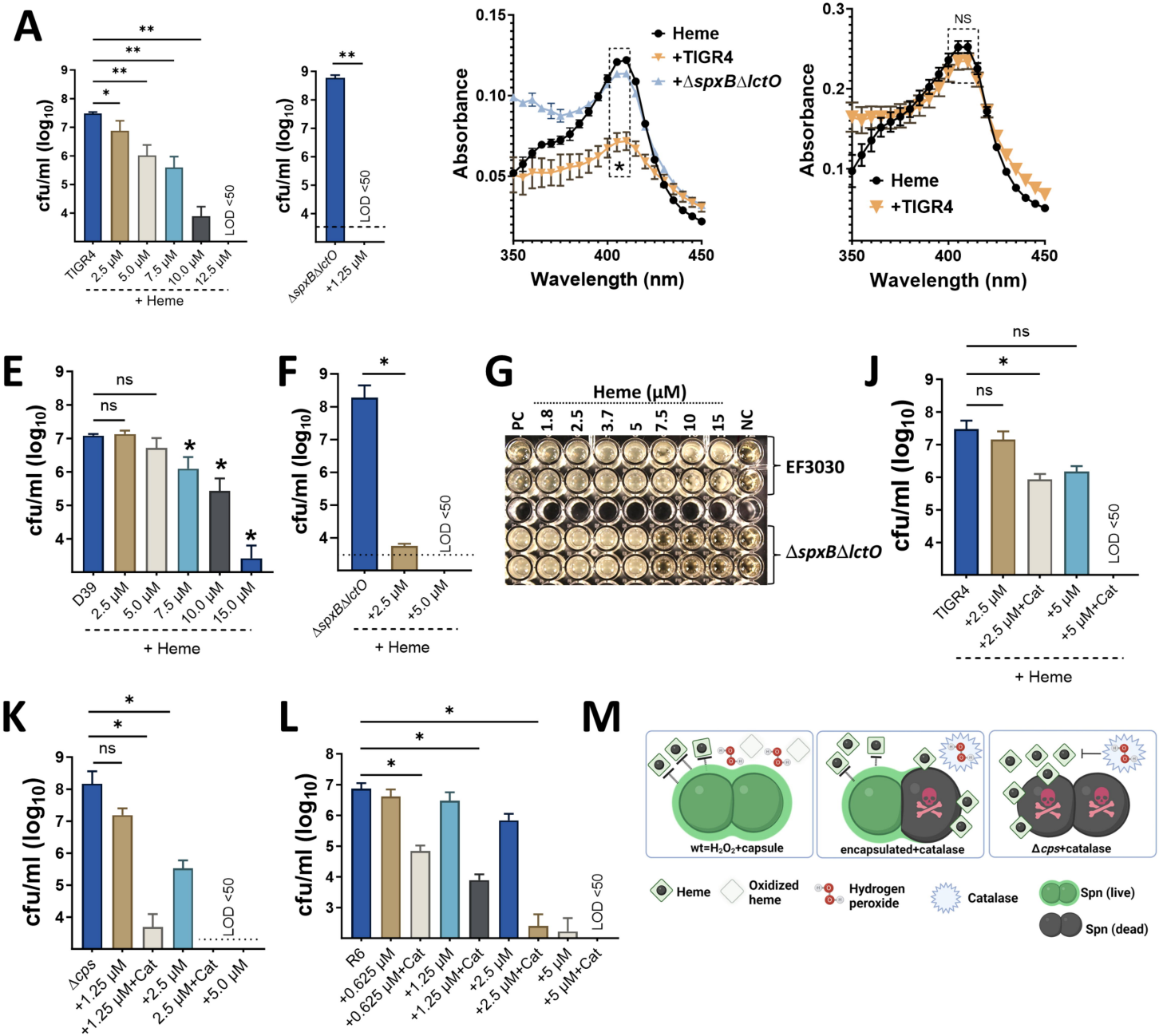
A
cfu/ml (log10)
TIGR4
2.5 µM
5.0 µM
7.5 µM
10.0 µM
12.5 µM
+ Heme
LOD <50
ΔspxBΔlctO
+1.25 µM
Absorbance
Wavelength (nm)
Heme
+TIGR4
+ΔspxBΔlctO
NS
E
D39
15.0 µM
ns
F
+2.5 µM
+5.0 µM
G
Heme (µM)
PC
1.8
2.5
3.7
5
7.5
10
15
NC
EF3030
ΔspxBΔlctO
J
+2.5 µM+Cat
+5 µM
+5 µM+Cat
K
Δcps
+1.25 µM+Cat
2.5 µM+Cat
L
R6
+0.625 µM
+0.625 µM+Cat
M
wt=H2O2+capsule
encapsulated+catalase
Δcps+catalase
Heme
Oxidized heme
Hydrogen peroxide
Catalase
Spn (live)
Spn (dead)